Single-Molecule Electrical Biosensors Based on Single-Walled Carbon Nanotubes

*Xuefeng Guo**

Interactions between biological molecules are fundamental to biology. Probing the complex behaviors of biological systems at the molecular level provides new opportunities to uncover the wealth of molecular information that is usually hidden in conventional ensemble experiments and address the "unanswerable" questions in the physical, chemical and biological sciences. Nanometer-scale materials are particularly well matched with biomolecular interactions due to their biocompatibility, size comparability, and remarkable electrical properties, thus setting the basis for biological sensing with ultra-high sensitivity. This brief review aims to highlight the recent progress of the burgeoning field of single-molecule electrical biosensors based on nanomaterials, with a particular focus on single-walled carbon nanotubes (SWNTs), for better understanding of the molecular structure, interacting dynamics, and molecular functions. The perspectives and key issues that will be critical to the success of next-generation single-molecule biosensors toward practical applications are also discussed, such as the device reproducibility, system integration, and theoretical simulation.

1. Introduction

In the past two decades, the discovery of abundant nanomaterials and advances in micro/nanofabrication technologies have opened up new avenues for developing novel biosensors, which hold great potential for applications in a wide variety of areas, ranging from diagnosis of life-threatening diseases, to detection of biological agents in warfare, or terrorist attacks.[1,2] In particular, various nanoscale electrical biosensors have been successfully developed based on carbon nanotubes,[3–5] nanowires,[6–9] nanopores,[10–12] nanoclusters,[13,14] and the emergent nanomaterial graphene.[15] Compared to conventional optical, biochemical, and biophysical methods, such as fluorescence/Raman spectroscopies, polymerase chain reactions (PCR) and enzyme-linked immunosorbent assays (ELISA), electrical biosensing based on nanomaterials offers unique advantages, such as simplicity, low-cost, portability, ultra-high sensitivity, excellent selectivity, and label-free real-time electrical detection in a non-destructive manner. The feasibility of integrating them with standard wafer-scale semiconductor processing techniques drives the field to move from fundamental problems in biological physics and bioengineering towards the development of practical biosensors.

The majority of nanomaterials-based electrical biosensors developed so far, however, are limited to simultaneous detection of large numbers of molecules that leads to the average properties. A key goal of modern bioscience is to monitor biomolecular interactions with high sensitivity and high selectivity in real time, with the ultimate aim of detecting single-molecule events in natural samples. Directly detecting the in situ activities of biological and chemical species at the single-molecule level can provide access to uncovering the incredible wealth of molecular information that is usually hidden in conventional ensemble experiments and addressing the previously "unanswerable" questions. Therefore, establishing a practical platform for achieving this is obviously of great importance to fundamental biology, diagnosis, and drug discovery. In this article, we aim to briefly summarize the recent progress of the burgeoning field of single-molecule electrical biosensors based on nanomaterials, with a focus on single-walled carbon nanotubes (SWNTs), for detecting biological interactions in real time, specifically DNA-protein interaction, DNA hybridization, enzymatic activity, and DNA translocation. The analysis of the stochastic processes, which are the signature of single-molecule observations that often happen in fluorescence blin king,[11,12,16–19] largely follows in the footsteps of this field with obviously some very different physical phenomena.

Prof. X. Guo
Center for Nanochemistry
Beijing National Laboratory for Molecular Sciences
State Key Laboratory for Structural Chemistry
of Unstable and Stable Species
College of Chemistry and Molecular Engineering
Department of Materials Science and Engineering
College of Engineering
Peking University
Beijing 100871, China
E-mail: guoxf@pku.edu.cn

DOI: 10.1002/adma.201301219

2. SWNTs for Biosensing

There has been an explosion of interest in use of one-dimensional nanostructured materials for the development of new nanoscale biosensors, and SWNTs are in the forefront of this explosion. This is because of their unique structural and physicochemical properties. First, it is known that the electrical properties of SWNTs depend strongly on their diameter and chirality. They can be either metallic conductors or semiconductors in terms of the structural chirality. This is useful for fabricating

SWNT-based nanosensors based on field-effect transistor (FET) layout,[3–5] where the physisorption of different molecules can modulate the nanotube conductance. Therefore, target biomolecules, which are in the close proximity of SWNTs, can potentially alter the electronic properties of SWNTs via one or more of the following mechanisms: 1) surface charge-induced gating, 2) charge transfer between SWNTs and biomolecules, 3) a scattering effect across SWNTs, and 4) Schottky barrier modification between SWNTs and metal electrodes. Second, SWNTs are well-ordered, hollow graphitic nanomaterials, formed by folding up a graphene sheet into a cylinder along a certain lattice vector.[20] This unique allotrope of carbon has the simplest chemical composition and atomic bonding configuration in a 1D manner that maximizes its surface-to-volume ratio. Each carbon atom on their surface is exposed to the environment and any tiny changes from the environment could cause drastic changes in their electrical properties, thus forming the basis for ultrasensitive biosensing. The third significant feature of SWNTs we should emphasize is that they are 1D conducting nanomaterials that are intrinsically the same size as biological entities, ensuring appropriate size compatibility between the detectors and the biological analytes. This size compatibility of SWNTs holds the promise of detecting single-molecule events. Fourth, SWNTs are molecular chemicals entirely composed of carbon atoms. As carbon is the backbone of all biomolecules and biostructures, SWNTs are naturally compatible with biomolecules. This also allows controlled functionalization to selectively immobilize bioaffinitive agents on their surfaces, and establishes efficient electrical communications with biological analytes through two approaches: non-covalent adsorption or wrapping of various bioaffinitive agents on their surfaces through hydrophobic interactions, and covalent attachment to the functional groups produced through chemical reactions on the π-conjugated skeleton of them. Ultimately, they are large enough and can be easily micro/nanofabricated on a large range of substrates. Therefore, in conjunction with their high conductivity, high chemical stability and easy availability through bottom-up approaches, all these advantages of SWNTs allow the development of new types of SWNT FET-based biosensors that, as we will show in the following sections, are starting to reach single-molecule detection.

3. Lithographic Method for Single-Molecule Biodetection

To achieve single-molecule electrical detection, covalently linking a single molecule of interest between two electrical conductors, which enables the electrical interrogation of that molecule as it dynamically interacts with the surrounding environment, is desirable. In practice, however, single-molecule devices remain exceedingly difficult to fabricate. Successes based on very small electrode gaps fabricated lithographically,[21] electrically,[22,23] or by scanning probe techniques[24,25] generally suffer from low fabrication throughput; electrical, mechanical, and chemical instabilities; poorly defined bonding to the molecule of interest; and, sometimes, inconclusive proof that only a single molecule is addressed. In the efforts to solve these issues, we recently described a system for measuring the conductivity of a single molecule covalently immobilized within a nanotube gap.[26] In this system, gaps are formed in SWNTs that can be reconnected by one or a few molecules attached to both sides of the gap through amide bond formation. This strategy allows molecules to be wired into electrodes by means of robust amide linkages, thus avoiding the assembly and reactivity problems which are commonly associated with dithiols between metal electrodes and form irreproducible electrical contacts. In addition, the devices are sufficiently robust that a wide range of chemistries and conditions could be applied, even in aqueous environments. By using this method, we have made molecular devices that are able to change their conductance as a function of pH, or switch their conductance when the bridging molecules are photoswitched.[27,28] These results form the basis for new types of chemical and biological sensors with single-molecule sensitivity.

As the first step towards biosensing, we developed a proof-of-principle strategy for achieving single-molecule biosensing from molecular electronic devices through the combination of programmed chemical reactivity and directed biological self-assembly.[29] In this study, each device was built from an individual SWNT that is oxidatively cut and chemically rewired together with a single conductive molecule. Because the current flow traverses a single molecule, the devices are sensitive to the local configuration and environment around the bridging molecule. One key advantage of this approach for biosensing is the ability to form a well-defined chemical linkage between a molecular wire and a probe molecule. Moreover, because each device is constructed from a single molecule, it has the capacity to monitor individual binding events. Using this approach, we were able to electrically sense oxime formation on the molecular bridge and to further detect the non-covalent binding between ligand and protein. We also demonstrated the use of biological assembly to localize individual nanoparticles at the molecular bridge, thus providing a means to construct and sense more complex nanostructures.

DNA possesses the maximal density of functionalities embedded in its double helical framework and superior sequence-specific self-assembly properties that make it a useful scaffold for the organization of molecules into higher-order nanostructures for the development of functional nanoscale

Dr. Xuefeng Guo received his Ph.D. in 2004 from the Institute of Chemistry, Chinese Academy of Sciences, Beijing. From 2004 to 2007, he was a postdoctoral research scientist at the Columbia University Nanocenter. He joined the faculty as a professor under "Peking 100-Talent" Program at Peking University in 2008. His research is focused on functional nanometer/molecular devices.

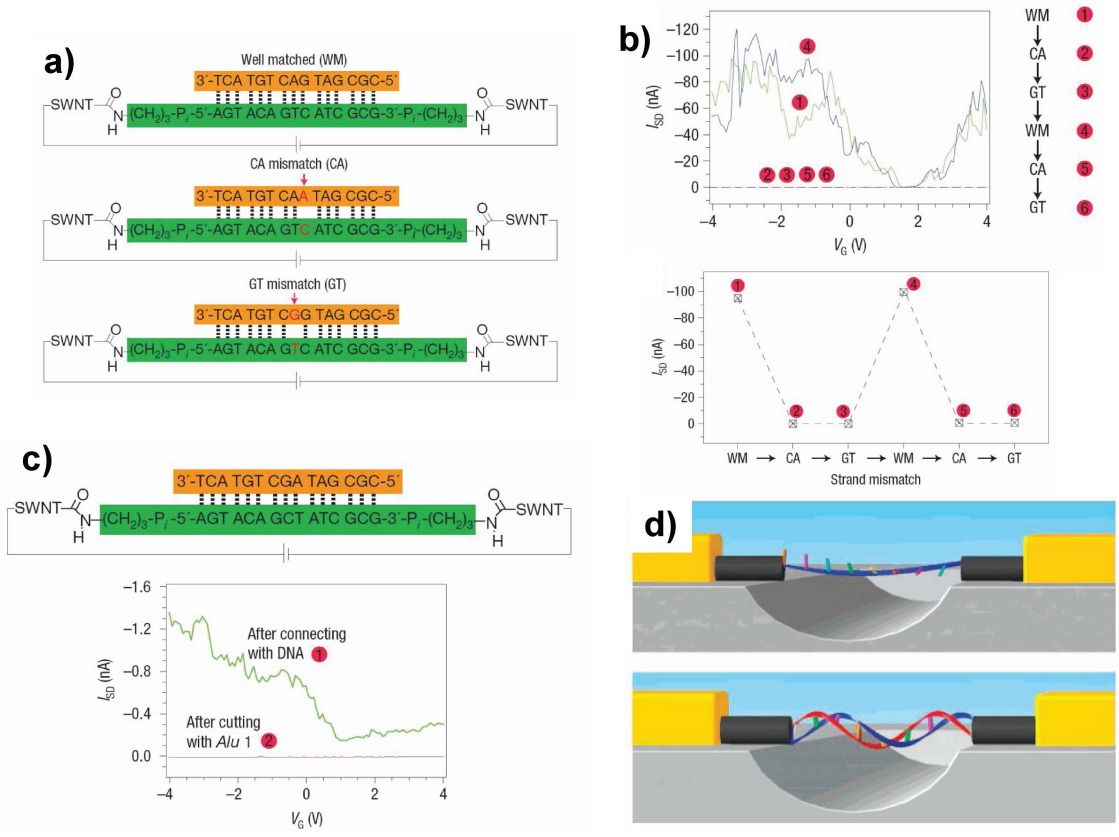

Figure 1. a) Effect of mismatches on DNA conductance. b) Source–drain current versus V_G at a constant source–drain voltage (50 mV) for a SWNT device taken through the sequence 1 through 6. The current levels for points 2, 3, 5, and 6 are ≈300 times lower. c) Source–drain current versus V_G at a constant source–drain voltage (50 mV) for a metallic SWNT device after cutting and reconnection with the shown DNA sequence (green curve: 1) and after reaction with *Alu*I (red curve: 2). Adapted with permission.[31] Copyright 2008, Nature Publishing Group. d) The upper figure represents an arbitrarily shaped ssDNA molecule, which is stretched and attached to a pair of functionalized SWNT electrodes in the presence of a dielectrophoresis field. The lower figure depicts a covalently attached dsDNA molecule, which has a definite conformation. Adapted with permission.[32] Copyright 2008, American Chemical Society.

devices and materials. In this context, one major effort is to transform DNA into a conductive material that would make a significant contribution to the development of the vibrant field of DNA-based molecular electronics. Numerous charge transport (CT) measurements on DNA strands bridging two electrodes have also been carried out in an effort to establish the conductivity of DNA.[30] These experiments demonstrate the high sensitivity of DNA charge transport to various factors, including the quality of the DNA-electrode interface, the base pair sequence, the charge injection into the molecule, or environmental effects (humidity, temperature, and counterions). Thus, in the conductivity measurements carried out so far, the integrity of the DNA was not well established, the connections to the duplex were not well defined, or the measurement was not definitively of a single DNA duplex. On the basis of the system we developed above, we recently demonstrated the first measurements of the conductivity of a single DNA duplex when it is wired into a carbon electrode through covalent bonds.[31] We modified DNA sequences with amines on either the 5′ terminus or both the 3′ and 5′ termini and coupled these to the single-walled carbon nanotube electrodes through amide linkages, enabling the electrical properties of complementary and mismatched strands to be measured (**Figure 1**a). We found that well-matched duplex DNA in the gap between the electrodes exhibited a resistance on the order of 1 MΩ and that a single GT or CA mismatch in a DNA 15-mer increased the resistance of the duplex ≈300-fold relative to a well-matched one (Figure 1a,b). Interestingly, when certain DNA sequences which are substrates for *Alu*I, a blunt end restriction enzyme, were oriented within this gap, this enzyme cut the DNA and eliminated the conductive path (Figure 1c), supporting the supposition that the DNA retains its native conformation and the corresponding biological activity when bridging the ends of SWNTs. These results prove that DNA molecules bridging nanodevices can surely serve as uniquely powerful reporters to transduce biochemical events into electrical signals at the single-molecule level, thereby opening up a new promising and exciting scientific research field that interfaces molecular nanodevices with biomacromolecules for a wide variety of potential applications. In another work, Roy et al. used focused ion beam (FIB) etching to make SWNT electrodes, where DNA molecules were suspended in the same chemical way through the nanotrench (Figure 1d).[32] They claimed that the presence of a nanotrench is important to eliminate the contribution of

the oxide surface to the CT through DNA molecules. They have tested 80 base pairs of single- and double-stranded DNA (ssDNA and dsDNA, respectively) of complex base sequences. Electrical measurements under vacuum showed that about a 25–40 pA current (at 1 V) was measured for the dsDNA molecule covalently attached to the SWNT electrode at its termini. In the absence of base pair stacking, a ssDNA carried a feeble current of ≈1 pA or less. Gate-voltage-dependent *I-V* characteristics revealed that the bridging dsDNA molecule acts as a p-type channel between SWNT source and drain electrodes.

On the basis of the above results, we noticed that unmodified DNA lacks sufficient electrical conductance, which might hamper its further application in nanoelectronics. To improve DNA conductivity, we described a method to make robust devices for directly measuring charge transport of metallo-DNA duplexes using single-molecule break junctions with SWNTs as point contacts (**Figure 2**a).[33] It was found that H–Cu^{2+}–H base pairs incorporated parallel to the neighboring natural base pairs in DNA could modulate its structural stability, rigidify π-stacking between DNA base pairs, and mediate the electronic coupling for hole transfer, thus favoring DNA charge transport. Therefore, for the first time, we experimentally support the idea that it is possible to enhance the electrical conductance of DNA by rational arrangement of multiple metal ions inside the core of the DNA base-pair stack (Figure 2c). In addition to this, we also found that the electrical properties of metallo-DNA-bridged devices can be efficiently switched on-and-off by sequentially alternating the treatments with EDTA and metal ions, thus forming a new type of chemical sensors for individual ions (Figure 2a).

After having understood CT properties of DNA molecules, we then turned our attention to creating an integrated system that can combine rapid real-time measurements with single-molecule sensitivity.[34] In this study, individual metallo-DNA aptamers, which are able to selectively and reversibly detect a target protein thrombin, were coupled with SWNTs as point contacts to form stable single-molecule devices (Figure 2d). At the initial stage, we treated the fresh aptamer-functionalized devices with thrombin. All the working devices showed the consistent conductance increases that originate from the enhanced DNA charge transfer because of the rigidification of DNA conformation by DNA-thrombin interactions (Figure 2e). To achieve real-time measurement, a repeating pattern that consists of 79 identical SWNT transistors by a double photolithographic process was designed and fabricated. Combining this design with microfluidics led to detecting protein and monitor stochastic DNA–protein interactions in real time (Figure 4f). Reversible and consistent conductance changes at different thrombin concentrations but without concentration dependence (from 2.6 fM to 2.6 pM and 2.6 nM; Figure 4f) were observed, therefore demonstrating the reproducibility and single-molecule sensitivity. Further delivery of elastase (3.4 nM) did not lead to any detectable conductance change in the same device. Control experiments using the device reconnected with another DNA, which could not bind human thrombin, showed negligible conductance change upon thrombin injection, thus proving the excellent selectivity. In another interesting work, the Nuckolls' group from Columbia University nicely created a device where the DNA is electronically integrated to serve as both the biological target and electrical transducer in a SWNT–DNA–SWNT device for detecting DNA binding and methylation by the methyltransferase M.SssI at the single-molecule level (Figure 2g).[35] They successfully demonstrated sequence-specific, reversible binding of M.SssI and protein-catalyzed methylation that alters the protein-binding affinity of the device. These results distinguished this method as a unique platform to achieve real-time, label-free, reversible detection of DNA–protein interactions and enzymatic activity with high selectivity and real single-molecule sensitivity. By using an electrical breakdown technique, Tang et al. demonstrated two-terminal planar type negative differential resistance (NDR) devices from SWNT-ferritin-SWNT junctions that exhibited reproducible NDR peaks with high current density.[36] The NDR behavior roots from active redox reactions of core transition metal ions in ferritin; hence, both positive and negative NDR peaks emerge upon bias voltage sweeps.

4. Point Functionalization for Single-Molecule Biodetection

To avoid the use of high-resolution lithographies, Goldsmith et al. recently developed an alternative electrochemical method to fabricate single-molecule electronic devices by creating single point defects in SWNTs in a controllable manner and then covalently binding biomolecules at the scattering site.[37] To prepare CVD-grown SWNTs for controlled oxidation, completed devices are mounted in an electrochemical cell and contacted by movable probe tips or fixed wirebonds (**Figure 3**a). They found that the electrochemical modification of SWNTs was electrolyte-dependent. Oxidation in bases and weak acids tended to be electrochemically irreversible. On the other hand, the strong acids, for example HNO_3, exhibited a very different behavior in which the application of a reductive potential after oxidation reverses the drop in conductance (*G*) (Figure 3b,c). In addition, they observed a substantial change in the electronic behavior of every metallic SWNT measured during redox cycles. Before oxidation, the *G* of a metallic SWNT is insensitive to a nearby gate electrode biased at voltage V_G. However, after a single redox cycle, metallic SWNTs became gate-sensitive probably because a point defect embedded in a metallic SWNT can cause this V_G modulation.

Dynamic investigations of the SWNT failure were performed in both reversible and irreversible electrolytes at the different biases. They found that *G* decreased continuously in time before stabilizing near 0.7 G_{init} (initial conductance) at precisely-controlled biases just below the threshold V_T, and more interestingly, *G* continued its decrease through a complex sequence of abrupt, discrete steps when coarse potentiostat control exceeded V_T, especially in the strong acids (Figure 3c). The intermediate terraces during oxidation exhibited excellent alignment (both step numbers and heights) with those during reduction. On the basis of these observations, they concluded that each step likely corresponds to the stochastic formation of a single covalent C–O bond between the SWNT and the electrolytes, in the same ways that such anions form adducts with the graphite basal plane. Further atomic force microscopic (AFM) characterizations did not show structural damage on these SWNTs in either the oxidized or reduced state.

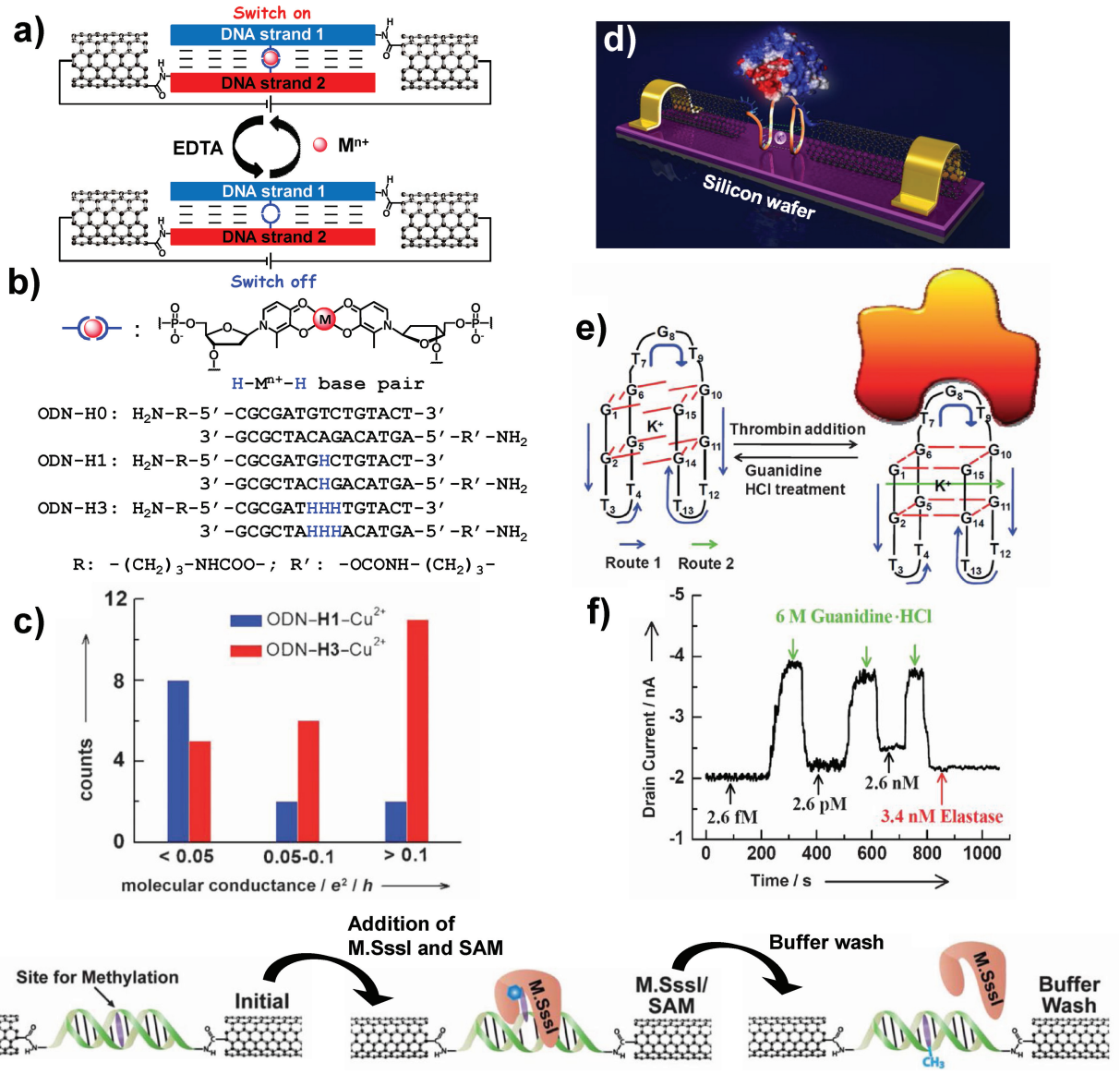

Figure 2. a) Schematic representation of the sensing process by sequentially alternating the treatments with EDTA and metal ions. b) The molecular structure of the Cu^{2+}-mediated base pair based on hydroxypyridone nucleobases (H) and the DNA sequences used in the study. c) Statistical conductance comparison between ODN–H1–Cu^{2+} and ODN–H3–Cu^{2+} duplexes. Adapted with permission.[33] Copyright 2011, Wiley-VCH. d) Representation of the device structure. e) Schematic representation of sensing mechanisms showing that protein binding rigidifies π-stacking in the G4 conformation, facilitating DNA CT. f) Current-versus-time data recorded for an Aptamer-rejoined device upon alternate additions of the thrombin Tris-HCl buffer solution at different concentrations (from 2.6 fM to 2.6 pM and 2.6 nM), the 6M guanidine HCl solution, and finally the elastase (3.4 nM) Tris-HCl buffer solution. Adapted with permission.[34] Copyright 2011, Wiley-VCH. g) Electrical detection of M.SssI binding at a DNA-bridged CNT device. Left: A DNA segment containing the M.SssI binding site (with target base to be methylated shown in purple) forms a conductive bridge between the two ends of a gap cut in a CNT device; Middle: Upon addition of M.SssI and SAM cofactor (represented by the blue hexagon), the methyltransferase binds the DNA at its recognition site, and flips the base to be methylated out of the DNA p-stack, thereby cutting off charge transport through the DNA. M.SssI remains bound with the base flipped even after the methylation reaction is complete; Right: Upon rinsing, M.SssI dissociates from the DNA; the methylated base re-inserts into the DNA p-stack and restores charge transport through the device. Adapted with permission.[35] Copyright 2011, Royal Chemical Society.

The presence of the resulted residual sites provides a chemical pathway for further sidewall functionalization with desired purposes. For example, they performed selective electrochemical deposition of Ni, a technique specially designed to label point defects on the basis of their enhanced reactivity, which makes the single site visible by scanning gate microscopy (SGM) as shown in Figure 3d. To achieve higher resolution, they finally treated redox-cycled SWNTs with 1-ethyl-3-(3-dimethylaminopropyl)carbodiimide (EDC) and n-hydroxysuccinimide (NHS) in an attempt to covalently link Au-labeled streptavidin to SWNT carboxyls. With the aid of additional $KMnO_4$ oxidation before EDC and NHS treatments, scanning

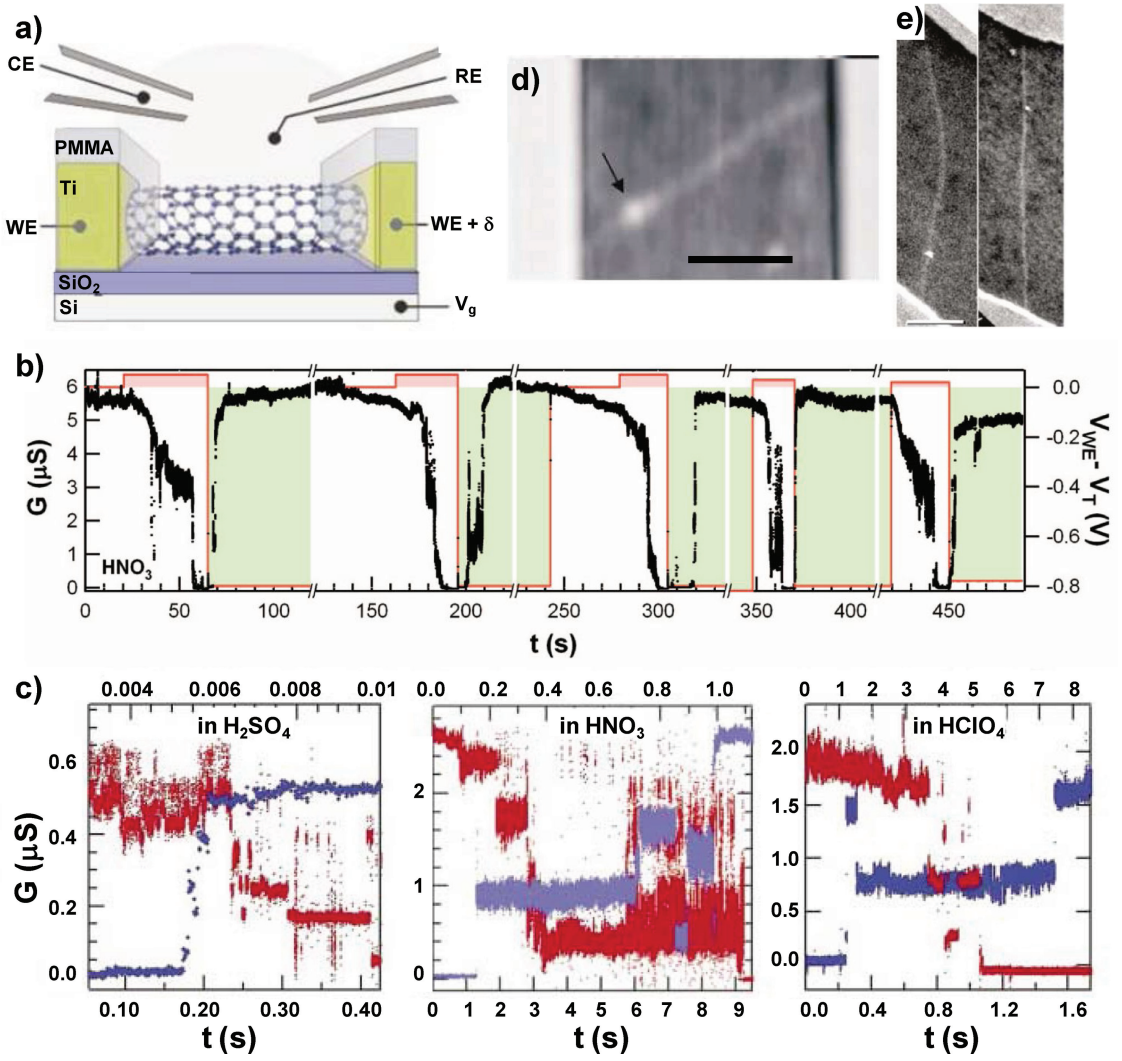

Figure 3. a) Schematic of SWNT circuit electrochemical modification. The dynamics of the circuit conductance *G* during modification differs between electrolytes. CE, counter electrode; RE, reference electrode; WE, working electrode. b) In strong acids, reduction results in nearly complete recovery of conductance and the same SWNT may be redox cycled multiple times. c) Higher-resolution oxidation (red, lower time scale) and reduction (blue, upper time scale) traces clarify a fine structure of abrupt jumps among metastable intermediate values. Three different strong acids shown here exhibit similar behaviors. All data in (b) and (c) were acquired at 100 kHz. The reduction portions of *G* in (b) have been scaled up 35% to adjust for the electrostatic gating that occurs at the reducing potential. d) SGM imaging shows that selective electrodeposition of Ni identifies this site as more chemically reactive than the rest of the SWNT. Scale bar, 500 nm. e) SEM images of SWNT devices incubated with streptavidin after controlled oxidation. Streptavidin covalently binds to each oxidation site, which has been activated by treatment with EDC and NHS. Each SWNT is visible because it is a conductor sitting on an insulating surface; the proteins are not visible but are labeled with 20-nm Au particles for imaging. Scale bar, 500 nm. Adapted with permission.[37] Copyright 2007, American Association for the Advancement Science.

electron microscopic (SEM) images after EDC and NHS treatments demonstrated successful attachements of both protein and Au nanoparticles (Figure 3e). Electrical characterization of these devices showed that *G* was critically dependent on the presence of the protein, consistent with the case of the Ni decorations, thus setting the foundation for further application in single-molecule biosensing. It should be mentioned that due to the real-time monitoring of conductance during defect generation, these point-functionalized SWNT FETs can be prepared with high yield. In their further study, they also demonstrated continuous, multihour monitoring of a single carboxylate group interacting with its immediate environment with high sensitivity (a conductance change of more than 100 nS for binding of a reactive carbodiimide), due to Coulomb interaction between the molecule and the defect that modulates scattering in the one-dimensional channel.[38]

By taking advantage of such point-functionalized SWNT devices, most recently, Sorgenfrei et al.[39] took a further step through a label-free field-effect-based approach to produce measurements of individual DNA hybridization kinetics and thermodynamics with high signal-to-noise ratio and bandwidth. They covalently attached a single-stranded probe DNA sequence (Probe 1: H_2N-5′-GGAAAAAAGG-3′), which was terminated with an amine group, to a carboxylic acid-functionalized point

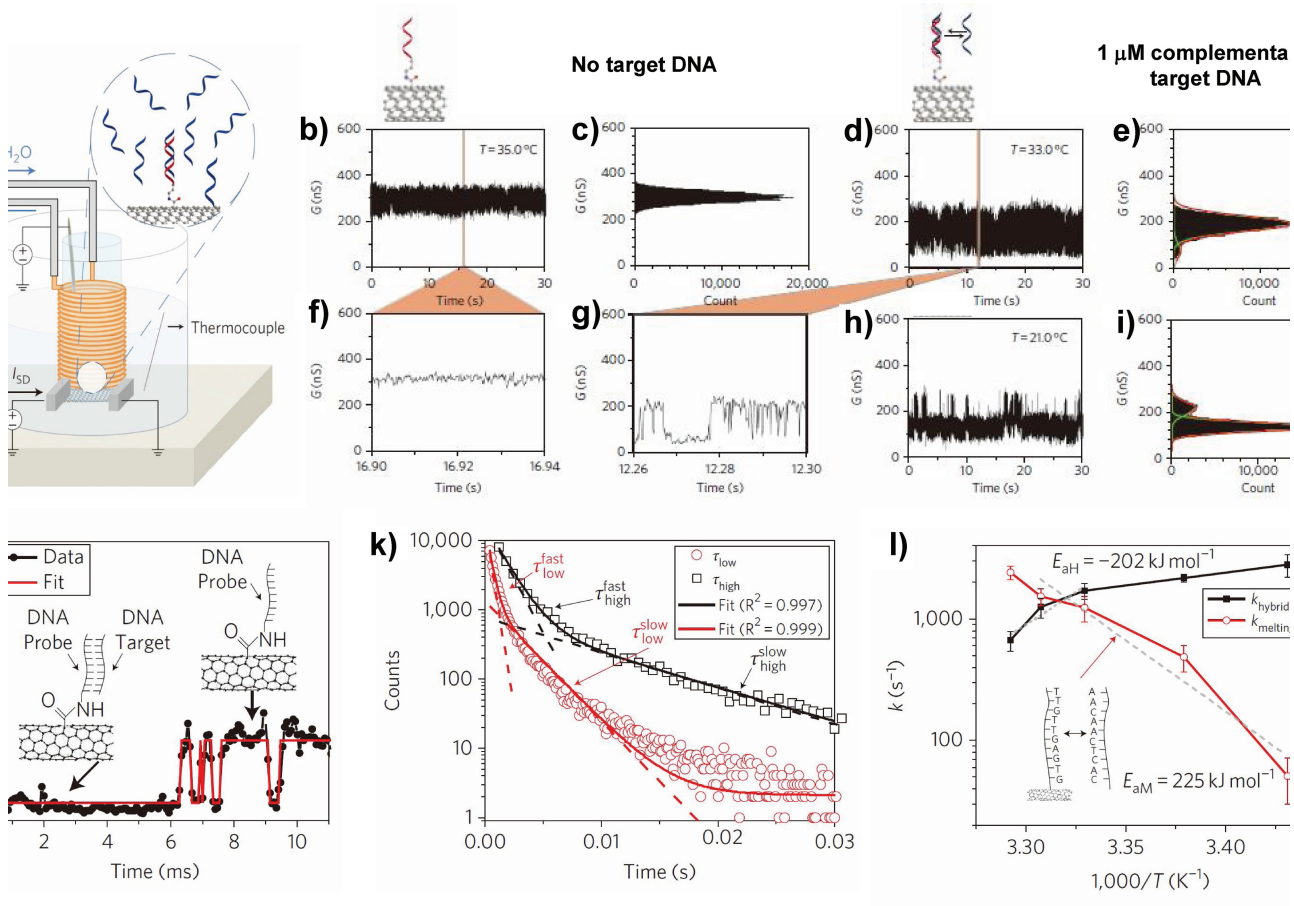

Figure 4. a) Schematic of the nanotube device used for studying the kinetics and thermodynamics of DNA hybridization (with an external circular heater/refrigerator to control temperature). b,d,h) Conductance recordings of devices over one 30 s interval with Probe 1 b) without exposure to complementary DNA target at 35.0 °C, d) after exposure to complementary DNA target at 33.0 °C, and h) after exposure to complementary DNA target at 21.0 °C. The source–drain bias is 100 mV and V_{Pt} is zero. c,e,i) Conductance-based histograms of time intervals shown in (b,d,h). The two levels in (e,i) are fit to Gaussian distributions. f,g) Representative short time interval (40 ms) for real-time conductance recording for probe only and after exposure to complementary target DNA. j) Conductance of a device with Probe 1 showing experiment data and idealized fits resulting from hidden-Markov-model analysis using vbFRET. Inset: associated bound and unbound states of the probe DNA. k) Example of double exponential fitting at 1 μM target concentration and 32 °C showing both fast and slow lifetimes for a device with a DNA probe H_2N-5′-GTGAGTTGTT-3′ (Probe 2). l) Arrhenius plot of another device with Probe 2. Error bars for the Arrhenius plots are calculated from at least sixteen different 15 s intervals. Adapted with permission.[39] Copyright 2011, Nature Publishing Group.

defect in a carbon nanotube through a standard amide-formation coupling reaction. After probe DNA attachment, these devices were used to study the kinetics and thermodynamics of DNA hybridization using the experimental setup shown in **Figure 4**a. Without the presence of target DNA, the devices didn't show any particular features in a conductance dominated by flicker (1/*f*) noise, as shown in Figure 4b,c. When the device was immersed in buffer containing complementary target DNA, however, the fluctuations developed into a two-level random telegraph signal (RTS), as shown in Figure 4d,e,h,i, with a conductance difference of ≈60–100 nS and with a signal-to-noise ratio of better than three over the 1/*f* noise background for a time interval of 30 s. The two conductance states showed strong temperature dependence (Figures 4d,e,h,i). The low-conductance state represented a device with duplex DNA and the high-conductance state represented a device with unbound probe DNA. This observation can be explained by the model that the device conductance is controlled by the combined but opposite effects: 1) target DNA binding that induces the scattering sites and thus the conductance decrease, and 2) Debye screening from dissolved solution counter-ions that results in the conductance increase. Further ionic screening experiments demonstrated that the fluctuation amplitude characterizing single-molecule interactions is dependent on charge in proximity to the defect site and buffer concentration, and increased by moving charges closer to the defect or by decreasing the buffer concentration.[40] In terms of the fact that the fluctuations are strongly fit to a two-level model, they concluded that only a single DNA interaction dominated the conductance modulation. By taking the ratio of the areas under the low- and high-conductance state curves, they calculated the melting temperature, which was slightly lower compared to the free DNA measured by UV–vis absorption probably due to interactions between the molecules and the surface.

Further kinetic investigations of the system as a function of temperature demonstrated non-Arrhenius behavior, in agreement with DNA hybridization experiments using fluorescence correlation spectroscopy. They extracted the dwell times in the high (τ_{high}) and low states (τ_{low}) in the presence of flicker noise by idealizing the transitions using a hidden Markov model (incorporated in the vbFRET software package) (Figure 4j). From this lifetime analysis, they determined that the dwell-time histograms could be best fit by a double exponential function with time constants, $\tau^{fast}{}_{low} < \tau^{slow}{}_{low}$ and $\tau^{fast}{}_{high} < \tau^{slow}{}_{high}$ (Figure 4k), which may be the result of two competing pathways for hybridization: three-dimensional diffusion or non-specific adsorption followed by surface diffusion. From the point of chemical kinetics, they expected the solution hybridization rate ($k_{hybridization}$) to be proportional to DNA target concentration (bimolecular process), and the solution melting rate ($k_{melting}$) to be independent of concentration (unimolecular process). Then, the Arrhenius plots achieved from a device with Probe 2 showed that the melting rates ($k_{melting}$) follow Arrhenius-like behavior and are very dependent on temperature, whereas the hybridization rates ($k_{hybridizing}$) have anti-Arrhenius behaviour and are only slightly temperature-dependent (Figure 4l). This anti-Arrhenius behavior yields a negative activation energy, which implies that the reaction rate decreases with increasing temperature and the free-energy barrier arises from a significant loss of entropy. They also found that the Arrhenius plot of the device with Probe 1, which consists of six adenine-thymine (A–T) base pairs that are enclosed by guanine-cytosine (G–C) bases, showed the different behavior for $k_{melting}$ with a sharp change in activation energy around the melting temperature probably due to bubble dynamics of the A–T regime of the DNA duplex. These results demonstrate that this methodology is powerful for the immediate exploration of applications in single-molecule studies with fast time resolution, such as label-free single-nucleotide polymorphism (SNP) detection, sequencing-by-synthesis (SBS), protein folding, and enzymatic activity.

5. Non-covalent Functionalization for Single-Molecule Biodetection

Although covalent sidewall modifications are often effective at installing functionality, they result in a change of carbon hybridization from sp^2 to sp^3, potentially leading to a partial impairment of conjugation with consequences for mechanical and/or electron-transport properties of SWNTs. On the other hand, non-covalent functionalization through π–π stacking or hydrophobic interaction, which is done in solution without introducing sp^3 centers, constitutes simple but invasive processes, preserving the primary structures of SWNTs along with their unique electronic and mechanical properties. It is because of these reasons that non-covalent functionalization has been extensively used to build optoelectronic devices and sensors.[3–5,41,42] By using this approach, recently, Choi et al. developed a method of tethering a single lysozyme molecule to a SWNT FET to produce a stable, high-bandwidth transducer for protein motion (**Figure 5**a).[43] In their experiments, the pyrenes were used to functionalize SWNTs through π–π stacking, and thus provided dilute anchor points for further derivatization of the surface. Then, individual T4 lysozyme (S90C) was successfully immobilized on the surface of SWNTs through covalent conjugation between a thiol of the cysteine unit from lysozyme and a pyrene maleimide anchor site in high yield (80%), as confirmed by AFM characterizations (Figure 5b), without the degradation of the lysozyme catalytic activity. After initial time-averaged, DC measurements, which proved these functional devices as chemical or biological sensors, they detailed further dynamic investigations that provided insights into conformational changes of the attached single protein. With one or more seconds of equilibration after peptidoglycan substrate was added, the fluctuations developed into a two-level RTS with a constant amplitude distribution but two distinct RTS fluctuation rates: the fast RTS state with a mean frequency of 316 Hz (Figure 5c) and the slow RTS state with a mean frequency of 15.4 Hz (Figure 5d). Each type of oscillation had a high and a low current state with characteristic durations τ_{hi} and τ_{lo}, respectively. Analysis of duration probability distributions showed that all four distributions were well fit by single exponential time constants for periods of analysis shorter than $\langle\tau_{mem}\rangle$ (the mean duration for each RTS), and analysis of much longer time periods resulted in biexponential distributions (Figure 5e,f). However, the fast and slow rates were sufficiently different so that they appeared as two distinguishable slopes as shown in Figure 5e,f. Figure 5e,f also provides a comparison of the probability distributions achieved at different pH values, showing that the pH dependence of lysozyme activity arises not from changes to its processive kinetics but rather from increasing time spent in either non-productive rapid motions or an inactive, closed conformation.

On the basis of data from dynamic experiments, they identified five independent parameters $\langle\tau_{hi}\rangle$ (the mean value of τ_{hi}), $\langle\tau_{lo}\rangle$ (the mean value of τ_{lo}), $\langle\tau_{mem}\rangle$, k (the mean turnover rate for the activity, $k = (\langle\tau_{hi}\rangle + \langle\tau_{lo}\rangle)^{-1}$), and ΔE (an energy separation determined by $\Delta E = k_B T \ln(\langle\tau_{hi}\rangle/\langle\tau_{lo}\rangle)$, all of which changed when the lysozyme switched from its fast RTS state to its slow RTS state. It was found that these parameters showed the pH dependence for a single lysozyme molecule. At pH 7, $\langle\tau_{mem}\rangle$ was nearly equal for the fast and the slow RTS state, and the percentage of the time (another independent parameter, a non-trivial combination of $\langle\tau_{mem}\rangle$ and their regularity) spent in either state approached 50%. At nonneutral pH values, however, multiple changes skewed this balance. For example, the increased time of inactive periods came at a cost to the percentage of time spent in the slow-switching RTS state. These parameters were very reproducible out of 50 single-molecule devices, although there were variations in the numerical rates observed. Considering the fact that lysozyme dynamics from previous ensemble and single-molecule FRET experiments were in excellent agreement with the observations from their nanocircuits, they concluded that the two-level electronic signal was caused by the lysozyme hinge motion, with slow RTS oscillations resulting from the transduction of catalytic turnover events and fast RTS oscillations corresponding to lysozyme's non-productive binding events. Further monitoring of the dynamic processivity of individual T4 lysozyme in the presence of either linear or crosslinked peptidoglycan substrates revealed that for both substrates, lysozyme exhibited processive low turnover rates of

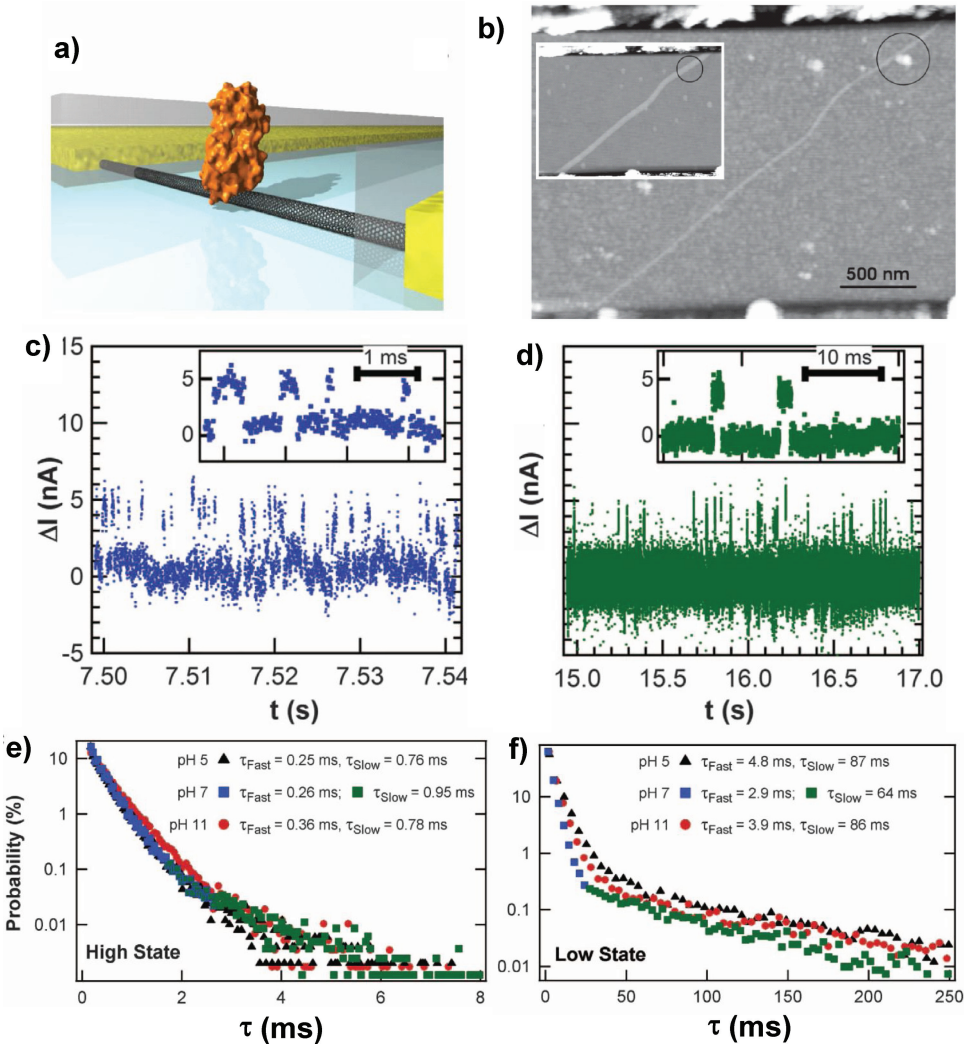

Figure 5. a) Schematic diagram of the single lysozyme being interrogated by a carbon nanocircuit. b) AFM topography of a SWNT FET before (inset) and after coating with the pyrene linker, lysozyme incubation, and washing to reduce non-specific binding. The circle highlights the point of lysozyme attachment. c) The faster RTS oscillates about 300 times per second. d) The slower RTS oscillates 15 times per second. The insets show individual switching events for each case. e,f) Probability distributions of continuous, 300-s data sets include as many as 105 transitions extending over many conversions between fast and slow RTS fluctuations. The inclusion of both fast and slow RTS sequences produces distinct, double-exponential distributions. e) Measurements at three different pH values show that the high-current state has almost no pH dependence. f) By contrast, the low-current state is at least 25% faster at pH 7 than at pH 5 or 11. Adapted with permission.[43] Copyright 2012, American Association for the Advancement Science.

20–50 s^{-1} and rapid (200–400 s^{-1}) non-productive motions.[44] However, the latter non-productive binding events occupied 43% of the enzyme time in the presence of the crosslinked peptidoglycan but only 7% with the linear substrate, thus distinguishing linear and crosslinked peptidoglycan substrates. In addition, they also found that lysozyme catalyzed the hydrolysis of glycosidic bonds to the end of the linear substrate but appeared to sidestep the peptide crosslinks to zigzag through the wild-type substrate.

The aforementioned consistence demonstrated that the nanocircuit architecture is complementary to traditional fluorescence techniques, but with the advantages that fluorescent labels are not required, the transduction mechanism does not bleach, and electronic bandwidths extend temporal resolution into the single-microsecond regime. As a result, the SWNT-lysozyme device data are more informative. Measurements of a long-duration $\langle\tau_{mem}\rangle$ support a processive catalytic mechanism in which each lysozyme hydrolyzes on average 100 glysodic bonds at 15-Hertz rates, before lysozyme returns to its non-productive, 330-Hertz hinge motion. The long-duration data sets also enabled analysis of the statistical variances for a single-step Poisson process, such as a statistical variance $\sigma^2 = \langle\tau\rangle^2$, and the normalized variance:

$$r = \frac{\sigma^2}{\langle t\rangle^2} = \frac{\sum_i (\tau_i - \langle\tau\rangle)^2}{\sum_i \tau_i^2} \quad (1)$$

from the τ_{hi} and τ_{lo} values. The analysis showed that the I_{lo} to I_{hi} transition has values of $r \approx 1$ and the reverse transition has values of $r < 1$. This proved that lysozyme forms a closed

conformation in a single step, but the transition back to its open configuration requires at least two steps. The reversible changes between two distinct states (open and closed conformations) moves lysozyme's charge residues back-and forth, therefore creating changes in electrostatic potentials that gate the channel conductance. The results demonstrate the tremendous potential of molecular electronics to uncover fundamental knowledge in biophysics.

6. Nanofluidic Method for DNA Translocation

SWNTs are allotropes of carbon with hollow cylindrical nanostructures, natural candidates as nanopores for analyzing molecular transport properties. Indeed, pressure-driven gas, water, and ion transport have been recorded through membranes composed of many multiwalled carbon nanotubes[45] or single-walled carbon nanotubes.[46,47] Molecular dynamics simulations predicted that both RNA[48] and DNA[49] could translocate through 1.5- to 2-nm diameter tubes. At this length scale, the passage of even a single molecule is able to generate a detectable change in the flow of ionic current through the pore, thus opening the possibility that some measurable translocation might occur at the much smaller fields that could be implemented in the laboratory. Recently, Liu et al. reported direct measurement of this translocation.[50]

In this study, a device where individual SWNTs with an outside diameter of 1 to 2 nm spans a barrier between two fluid reservoirs was designed and fabricated (**Figure 6**a). This arrangement makes it possible to detect signals from the translocation of a single molecule and to correlate transport with the properties of individual SWNTs. With electron-beam lithography, they formed fluid reservoirs along the path of chosen tubes and applied mild oxygen plasma etching with care to remove the exposed parts of the SWNT, leaving the SWNT under the barrier intact and ruling out the possibility of current leakages from the interface between SWNTs and photoresists. Then, the fluidic pathway was completed by placing a poly(dimethylsiloxane) (PDMS) cover on top of the chip (Figure 6b). They first measured the ionic conductance of 1 M KCl solution through SWNTs, showing that the SWNTs with the highest ionic conductance are all metallic (Figure 6c). Control experiments using a conducting tube suspended in a potential gradient in an electrolyte as a bipolar electrode showed that enormous fields were required to drive electrochemical processes at the ends of a bipolar carbon nanotube electrode, thus precluding the possibility of electrochemical currents stemming from reduction and oxidation reactions at the end of metallic tubes. One possible mechanism for the large ionic currents is that the selective filtering of anions or cations owing to charged end groups can result in a net excess concentration of one charge inside the tube which, in turn, drives an electroosmotic current. Molecular dynamics simulations further showed that both anions and cations can be driven in the same direction by an extremely large electroosmotic flow, but only the charge imbalance inside the tube results in a net ionic current. Because the mechanism of charge accumulation is complex and involves both charged end groups and the electronic properties of the SWNT, they have not yet developed a quantitative model for it.

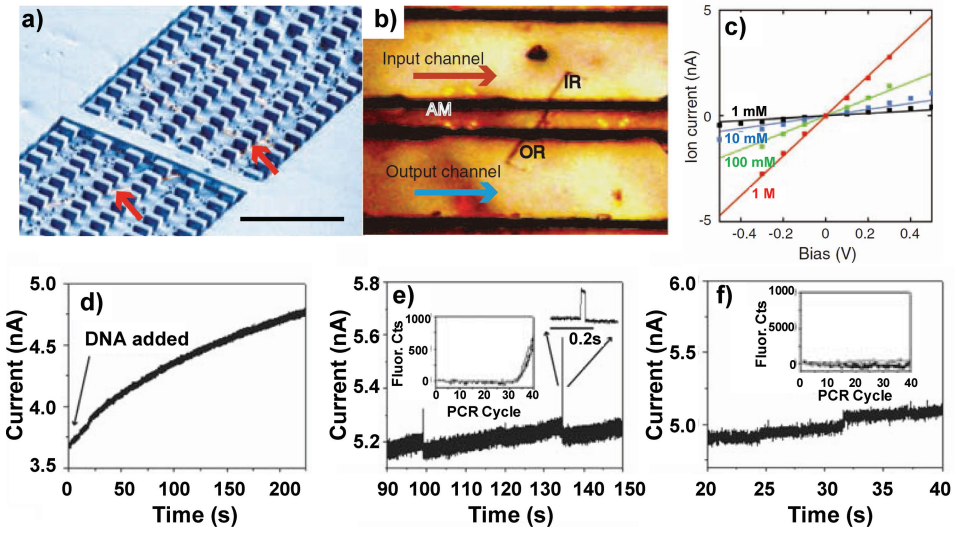

Figure 6. a) A single nanopore device was fabricated using individual CVD-grown high-quality SWNTs. Photoresist pillars in the reservoir support the PDMS cover. Details for device fabrications can be found elsewhere.[45] b) Optical image taken through a PDMS cover. The reservoirs (IR, input; OR, output) span the barrier between PDMS channels at an angle of about 60°. AM marks the location of one set of alignment markers. c) Current versus voltage applied to Ag/AgCl reference electrodes for a 2-mm long, 1.7-nm diameter SWCNT for various concentrations of KCl electrolyte as marked. d) After DNA addition, current slowly increased. e) 5 min after addition of 0.1-nM 60-nt DNA, large positive current spikes appeared. These spikes were followed by a drop in baseline over a period of a second or so and then by a gradual rise leading to the next spike. f) Data from a tube that showed both a current increase on DNA addition and baseline fluctuations but no spikes. No translocation was detected by PCR. The insets in (e) and (f) show the fluorescence signal from double-stranded DNA dye labels as a function of the PCR cycle number for samples collected from these particular runs. Adapted with permission.[50] Copyright 2010, American Association for the Advancement Science.

After having understood the ionic conductance of SWNT nanopores, they then turned the attention to studying DNA translocation through SWNTs. In the subset of high current tubes, they first observed a slow increase in the background current (Figure 6d). After some time, which varied from a few to tens of minutes, depending on the DNA concentration in the input reservoir, large transient increases ("spikes" with large fluctuations) were observed (Figure 6e), but only occurring only in tubes with conductances (before DNA addition) of >2 nS. In combination with positive quantitative polymerase chain reaction (QPCR) experiments, these results strongly proved that DNA was translocated through SWNTs manifesting the large spikes. QPCR also provided a measure of the number of molecules collected. They found that all the working devices appeared to pass more than one molecule per spike. For example, two out of six working devices passed at least 30 to 40 molecules for each spike. This is probably because the tube fills entirely with DNA, the spike signaling the cooperative emptying (or possibly filling) of the tube. From the dada of the spike duration and amplitude, they analyzed the charge contained in each spike. The value is remarkably large, at about 1 pC or 10^7 electrons in each spike. This might be due to a consequence of additional mobile ions brought into the channel by DNA molecules and/or large changes in the polarization outside the tubes. Control experiments using "failed" devices (i.e., lacking the CNT and deliberately overetched) that displayed leakage current showed evidence of DNA in the output well, but none displayed spikes (Figure 6f). On the basis of these observations, they concluded that carbon nanotubes simplify the construction of nanopores, permit new types of electrical measurements, and may open avenues for control of DNA translocation or sequencing at the molecular level.

7. Summary and Outlook

Recent advances in the burgeoning area of single-molecule biosensing based on carbon nanotube systems have been summarized here. By taking advantage of the unique structural, physical and electrical properties of SWNTs, four different sophisticated strategies have been developed to create single-molecule devices for directly detecting DNA hybridization, DNA-protein interaction, enzymatic activity, and DNA translocation in real time, which reaches real single-molecule sensitivity. Compared to conventional ensemble experiments, single-molecule studies provide new opportunities to uncover usually-hidden molecular information and address the critical issues in the physical, chemical and biological sciences. In addition to the examples discussed here, single-molecule biosensors have the powerful capabilities to probe many other complex behaviors of biological systems as diverse as protein folding, single-nucleotide polymorphism (SNP), enzymatic activity, DNA sequencing, cellular communication, and other tissue functions, suggesting a thriving research field and countless applications in a wide variety of areas, for example, clinic diagnostics, environment preservation, health improvement, drug discovery, national defense, and bioterrorism prevention.

Despite this promise, single-molecule studies based on SWNTs still face considerable challenges before they can realize their full commercial potential. One of the major challenges primarily stems from the device-to-device heterogeneity in their baseline electronic properties. This is because of the lack of precise diameter and chirality control for SWNTs through bottom-up approach. Developing a reliable and scalable fabrication technique and methodology for mass-producing identical SWNT arrays and integrating individual SWNTs into functional single-molecule devices with high yields are some of the technical issues to be addressed in future. The next problem arises from the lack of system integration. Most of the studies reported in the literature used a sample delivery system, such as a syringe pump, which was neither integrated to the sensing platform, nor to the readout module. Furthermore, without exception so far, all the measurements were carried out in ideal media, such as pure buffer solutions. The real physiological sample is far more complex and will definitely introduce a range of interfering and fouling effects. In addition, the development of fabricating parallel and integrated sensor arrays with specific functionalities in selective areas by either sophisticated device engineering or chemical methods, which is suitable for biosensing in a multiplexed fashion, remains challenging. As single-molecule researches continue to grow, clearly, another critical component that will become increasingly important is the routine and synergistic side-by-side use of theory in the planning and analysis of single-molecule experiments. Side-by-side use of molecular theory and simulations is equally important to help enhance much better understanding of the molecular system under consideration, and therefore guide and complement single-molecule experiments.

Although we are focusing on SWNTs, other nanomaterials could be used to create nanoscale biosensors for single-molecule studies. For example, graphene, a new allotrope of carbon made of sp^2-hybridized carbon atoms arranged in a honeycomb lattice, is an ideal two-dimensional system for developing new types of nanoscale biosensors.[51,52] Recently, the increasing swell of interest in using graphene for biosensing seems to exceed the use of SWNTs in biosensing. Other low-dimensional semiconducting materials, such as silicon nanowires because of their superior structural and electrical properties with precise contrallability, easy availability through bottum-up approaches, and the capability of the integration with the exisitng silicon industry, have also demonstrated great potential for single-molecule biosensing.[53–60] To fully utilize these disticnt and complementary nanomaterials, it is of crucial importance to develop creative strategies to reproducibly make functional molecular electronic devices in large number in order to directly acquire the intrinsic information of biological systems with real-time capability and single-molecule sensitivity in a non-destructive manner.

This Progress Report discusses the current interests and efforts in interfacing single-molecule electronics with biology. We can expect that single-molecule studies, as required by the diverse expertise critical to making key advances in the field, will foster truly excellent collaboration bringing biology, chemistry and physics together, thus forcing the rapid development of the field.

Acknowledgements

We acknowledge primary financial support from MOST (2012CB921404) and NSFC (21225311, 51121091 and 2112016).

Received: March 16, 2013
Published online: May 21, 2013

[1] N. L. Rosi, C. A. Mirkin, *Chem. Rev.* **2005**, *105*, 1547–1562.
[2] J. W. Liu, Z. H. Cao, Y. Lu, *Chem. Rev.* **2009**, *109*, 1948–1998.
[3] B. L. Allen, P. D. Kichambare, A. Star, *Adv. Mater.* **2007**, *19*, 1439–1451.
[4] G. Gruner, *Anal. Bioanal. Chem.* **2006**, *384*, 322–335.
[5] S. Liu, Q. Shen, Y. Cao, L. Gan, Z. Wang, M. L. Steigerwald, X. Guo, *Coord. Chem. Rev.* **2010**, *254*, 1101–1116.
[6] F. Patolsky, G. Zheng, C. M. Lieber, *Anal. Chem.* **2006**, *78*, 4260–4269.
[7] K.-I. Chen, B.-R. Li, Y.-T. Chen, *Nano Today* **2011**, *6*, 131–154.
[8] A. Mulchandani, N. V. Myung, *Curr. Opin. Biotechnol.* **2011**, *22*, 502–508.
[9] N. S. Ramgir, Y. Yang, M. Zacharias, *Small* **2010**, *6*, 1705–1722.
[10] S. Howorka, Z. Siwy, *Chem. Soc. Rev.* **2009**, *38*, 2360–2384.
[11] H. Bayley, L. Jayasinghe, *Mol. Membr. Biol.* **2004**, *21*, 209–220.
[12] H. Bayley, P. S. Cremer, *Nature* **2001**, *413*, 226–230.
[13] L. Soleymani, Z. C. Fang, E. H. Sargent, S. O. Kelley, *Nat. Nanotechnol.* **2009**, *4*, 844–848.
[14] X. Chen, Z. Guo, G.-M. Yang, J. Li, M.-Q. Li, J.-H. Liu, X.-J. Huang, *Mater. Today* **2010**, *13*, 28–41.
[15] W. Yang, K. R. Ratinac, S. P. Ringer, P. Thordarson, J. J. Gooding, F. Braet, *Angew. Chem. Int. Ed.* **2010**, *49*, 2114–2138.
[16] K. T. Shimizu, R. G. Neuhauser, C. A. Leatherdale, S. A. Empedocles, W. K. Woo, M. G. Bawendi, *Phys. Rev. B* **2001**, *63*, 205316.
[17] R. G. Neuhauser, K. T. Shimizu, W. K. Woo, S. A. Empedocles, M. G. Bawendi, *Phys. Rev. Lett.* **2000**, *85*, 3301–3304.
[18] W.-T. Yip, D. Hu, J. Yu, D. A. V. Bout, P. F. Barbara, *J. Phys. Chem. A* **1998**, *102*, 7564–7575.
[19] P. F. Barbara, A. J. Gesquiere, S.-J. Park, Y. J. Lee, *Acc. Chem. Res.* **2005**, *38*, 602–610.
[20] H. Dai, *Acc. Chem. Res.* **2002**, *35*, 1035–1044.
[21] A. A. Tseng, A. Notargiacomo, T. P. Chen, *J. Vac. Sci. Technol. B* **2005**, *23*, 877–894.
[22] H. Park, A. K. L. Lim, A. P. Alivisatos, J. Park, P. L. McEuen, *Appl. Phys. Lett.* **1999**, *75*, 301–303.
[23] D. R. Strachan, D. E. Smith, D. E. Johnston, T. H. Park, M. J. Therien, D. A. Bonnell, A. T. Johnson, *Appl. Phys. Lett.* **2005**, *86*, 043109.
[24] N. J. Tao, *J. Mater. Chem.* **2005**, *15*, 3260–3263.
[25] W. Ho, *J. Chem. Phys.* **2002**, *117*, 11033–11061.
[26] X. Guo, J. P. Small, J. E. Klare, Y. L. Wang, M. S. Purewal, I. W. Tam, B. H. Hong, R. Caldwell, L. M. Huang, S. O'Brien, J. M. Yan, R. Breslow, S. J. Wind, J. Hone, P. Kim, C. Nuckolls, *Science* **2006**, *311*, 356–359.
[27] A. K. Feldman, M. L. Steigerwald, X. Guo, C. Nuckolls, *Acc. Chem. Res.* **2008**, *41*, 1731–1741.
[28] X. Guo, C. Nuckolls, *J. Mater. Chem.* **2009**, *19*, 5470–5473.
[29] X. Guo, A. Whalley, J. E. Klare, L. Huang, S. O'Brien, M. Steigerwald, C. Nuckolls, *Nano Lett.* **2007**, *7*, 1119–1122.
[30] J. C. Genereux, J. K. Barton, *Chem. Rev.* **2010**, *110*, 1642–1662.
[31] X. Guo, A. A. Gorodetsky, J. Hone, J. K. Barton, C. Nuckolls, *Nat. Nanotechnol.* **2008**, *3*, 163–167.
[32] S. Roy, H. Vedala, A. D. Roy, D. H. Kim, M. Doud, K. Mathee, H. K. Shin, N. Shimamoto, V. Prasad, W. B. Choi, *Nano Lett.* **2008**, *8*, 26–30.
[33] S. Liu, G. H. Clever, Y. Takezawa, M. Kaneko, K. Tanaka, X. Guo, M. Shionoya, *Angew. Chem. Int. Ed.* **2011**, *50*, 8886–8890.
[34] S. Liu, X. Y. Zhang, W. X. Luo, Z. X. Wang, X. Guo, M. L. Steigerwald, X. H. Fang, *Angew. Chem. Int. Ed.* **2011**, *50*, 2496–2502.
[35] H. Wang, N. B. Muren, D. Ordinario, A. A. Gorodetsky, J. K. Barton, C. Nuckolls, *Chem. Sci.* **2012**, *3*, 62–65.
[36] Q. Tang, H. K. Moon, Y. Lee, S. M. Yoon, H. J. Song, H. Lim, H. C. Choi, *J. Am. Chem. Soc.* **2007**, *129*, 11018–11019.
[37] B. R. Goldsmith, J. G. Coroneus, V. R. Khalap, A. A. Kane, G. A. Weiss, P. G. Collins, *Science* **2007**, *315*, 77–81.
[38] B. R. Goldsmith, J. G. Coroneus, A. A. Kane, G. A. Weiss, P. G. Collins, *Nano Lett.* **2008**, *8*, 189–194.
[39] S. Sorgenfrei, C. Y. Chiu, R. L. Gonzalez, Y. J. Yu, P. Kim, C. Nuckolls, K. L. Shepard, *Nat. Nanotechnol.* **2011**, *6*, 125–131.
[40] S. Sorgenfrei, C. Y. Chiu, M. Johnston, C. Nuckolls, K. L. Shepard, *Nano Lett.* **2011**, *11*, 3739–3743.
[41] R. J. Chen, Y. Zhang, D. W. Wang, H. J. Dai, *J. Am. Chem. Soc.* **2001**, *123*, 3838–3839.
[42] S. Liu, J. Li, Q. Shen, Y. Cao, X. Guo, G. Zhang, C. Feng, J. Zhang, Z. Liu, M. L. Steigerwald, D. Xu, C. Nuckolls, *Angew. Chem. Int. Ed.* **2009**, *48*, 4759–4762.
[43] Y. Choi, I. S. Moody, P. C. Sims, S. R. Hunt, B. L. Corso, I. Perez, G. A. Weiss, P. G. Collins, *Science* **2012**, *335*, 319–324.
[44] Y. Choi, I. S. Moody, P. C. Sims, S. R. Hunt, B. L. Corso, D. E. Seitz, L. C. Blaszcazk, P. G. Collins, G. A. Weiss, *J. Am. Chem. Soc.* **2012**, *134*, 2032–2035.
[45] B. J. Hinds, N. Chopra, T. Rantell, R. Andrews, V. Gavalas, L. G. Bachas, *Science* **2004**, *303*, 62–65.
[46] J. K. Holt, H. G. Park, Y. M. Wang, M. Stadermann, A. B. Artyukhin, C. P. Grigoropoulos, A. Noy, O. Bakajin, *Science* **2006**, *312*, 1034–1037.
[47] X. C. Qin, Q. Z. Yuan, Y. P. Zhao, S. B. Xie, Z. F. Liu, *Nano Lett.* **2011**, *11*, 2173–2177.
[48] I. C. Yeh, G. Hummer, *Proc. Natl. Acad. Sci. USA* **2004**, *101*, 12177–12182.
[49] Y. H. Xie, Y. Kong, A. K. Soh, H. J. Gao, *J. Chem. Phys.* **2007**, *127*, 225101.
[50] H. T. Liu, J. He, J. Y. Tang, H. Liu, P. Pang, D. Cao, P. Krstic, S. Joseph, S. Lindsay, C. Nuckolls, *Science* **2010**, *327*, 64–67.
[51] T. Cohen-Karni, Q. Qing, Q. Li, Y. Fang, C. M. Lieber, *Nano Lett.* **2010**, *10*, 1098–1102.
[52] N. Mohanty, V. Berry, *Nano Lett.* **2008**, *8*, 4469–4476.
[53] F. Patolsky, G. Zheng, O. Hayden, M. Lakadamyali, X. Zhuang, C. M. Lieber, *Proc. Natl. Acad. Sci. USA* **2004**, *101*, 14017–14022.
[54] F. Shen, J. Wang, Z. Xu, Y. Wu, Q. Chen, X. Li, X. Jie, M. Yao, X. Guo, T. Zhu, *Nano Lett.* **2012**, *12*, 3722–3730.
[55] X. Duan, R. Gao, P. Xie, Cohen-Karni. Tzahi, Q. Qing, H. S. Choe, B. Tian, X. Jiang, C. M. Lieber, *Nat. Nanotechnol.* **2012**, *7*, 174–179.
[56] P. Xie, Q. Xiong, Y. Fang, Q. Qing, C. M. Lieber, *Nat. Nanotechnol.* **2012**, *7*, 119–125.
[57] F. Shen, M. Tan, Z. Wang, M. Yao, Z. Xu, Y. Wu, J. Wang, X. Guo, T. Zhu, *Environ. Sci. Technol.* **2011**, *45*, 7473–7480.
[58] Z. Jiang, Q. Qing, P. Xie, R. X. Gao, C. M. Lieber, *Nano Lett.* **2012**, *12*, 1711–1716.
[59] X. P. A. Gao, G. F. Zheng, C. M. Lieber, *Nano Lett.* **2010**, *10*, 547–552.
[60] G. S. Kulkarni, Z. H. Zhong, *Nano Lett.* **2012**, *12*, 719–723.